Available online at www.sciencedirect.com
SCIENCE DIRECT®
International Journal of Heat and Fluid Flow 25 (2004) 262–273
International Journal of HEAT AND FLUID FLOW
www.elsevier.com/locate/ijhff

A study of the effects of heater size, subcooling, and gravity level on pool boiling heat transfer

Christopher D. Henry, Jungho Kim *

Department of Mechanical Engineering, University of Maryland, 3181 Glenn L Martin Hill, College Park, MD 20742, USA

Abstract

Pool boiling heat transfer measurements from different heater sizes were obtained in low-g (0.01 ± 0.025 g) and high-g (1.7 ± 0.5 g) aboard the KC-135 aircraft. Boiling on three heaters of different size (0.65, 2.62, 7.29 mm^2) was studied. Control circuitry was used to maintain an isothermal boundary condition on the heater surface while the power dissipated by the heater was measured. Steady-state boiling data in low-g and high-g were obtained for various bulk fluid subcoolings and wall superheats. For the two larger heaters in low-g, critical heat flux (CHF) increased with increasing bulk subcooling and is significantly smaller than the CHF obtained in high-g. Satellite bubble coalescence with the primary bubble was the mechanism by which CHF occurred in low-g for larger heaters. At high subcoolings and wall superheats, above that of which CHF occurred, the onset of strong thermocapillary convection caused an increase in heat transfer above CHF. For the small heater in low-g, bulk subcooling had a negligible impact on boiling performance and a characteristically low heat flux was observed for the CHF. In high-g, boiling on heaters roughly the size of the bubble departure diameter was dominated by surface tension and characterized by a very low bubble departure frequency. For larger heaters in high-g, bubble departure frequency decreased with increasing subcooling but time and surface averaged heat transfer remained unaffected.

Keywords: Microgravity; Boiling; Microheater; Subcooling; Heater size

1. Introduction

Future space technologies are anticipated to dissipate large amounts of power while placing an emphasis on miniaturization. Such design characteristics, representative of today's high-speed electronics and cutting edge MEMS devices, raise significant thermal issues that are not easily solved using contemporary thermal management solutions. Boiling heat transfer has gained considerable attention over the years due to the large dissipative heat flux that can be achieved with relatively small temperature differences. Such characteristics have led to research efforts aimed at quantifying boiling behavior at the small scale in variable gravitational environments. A firm understanding of the boiling mechanisms in a host of operational environments is paramount to designing robust, efficient, economical, and reliable solutions for the future.

Boiling heat transfer has traditionally been thought of as a combination of free convection, vapor–liquid exchange, microconvection, transient conduction, and latent heat of vaporization. Vapor bubble dynamics associated with nucleation, bubble growth, departure, collapse, and subsequent rewetting of the heater surface characterize the classical ebullition cycle which constitutes the central mechanism of heat transfer from a superheated wall during nucleate boiling in earth gravity. Many researchers have characterized heat transfer from heater sizes much larger than the capillary length scale, L_b.

$$L_b = \sqrt{\frac{\sigma}{g(\rho_l - \rho_v)}} \tag{1}$$

Such work has laid the foundation for the classical boiling curve and its constituent boiling regimes.

Experiments first conducted by Gunther and Kreith (1956) showed the majority of heat transfer during subcooled nucleate pool boiling can be attributed to

* Corresponding author. Tel.: +1-301-405-5437; fax: +1-301-314-9477.
E-mail addresses: cdh@wam.umd.edu (C.D. Henry), kimjh@eng.umd.edu (J. Kim).

0142-727X/$ - see front matter © 2003 Elsevier Inc. All rights reserved.
doi:10.1016/j.ijheatfluidflow.2003.11.019

Nomenclature

A_i	area of individual heater element (m^2)
A_h	total heater area (m^2)
α	thermal diffusivity (m^2s)
Bo	Bond number
C_0	0.1
c_p	specific heat of liquid (J/kg K)
C_{sf}	Rohsenhow constant
D_d	bubble departure diameter (m)
f	bubble departure frequency (Hz)
g	gravitational constant (m/s^2)
h	heat transfer coefficient (W/m^2 K)
h_{fg}	heat of vaporization (J/kg)
k	thermal conductivity (W/m K)
L_b	capillary length (m)
λ_c	critical wavelength (m)
λ_d	most dangerous wavelength (m)
L_h	heater length (m)
M	molecular weight (kg/mol)
m	0.12–0.2 $\log_{10} R_p$
n	number of powered heaters
μ	dynamic viscosity of liquid (N s/m^2)
Nu	Nusselt number
P	pressure (N/m^2)
P_c	critical pressure (N/m^2)
Pr	Prandtl number of liquid
P_r	reduced pressure
$q''_{CHF,sub}$	critical heat flux, subcooled bulk conditions (W/m^2)
$q''_{CHF,sat}$	critical heat flux, saturated bulk conditions (W/m^2)
q''	heat flux (W/m^2)
$q_{raw,i}$	heat flux from heater element i (W/m^2)
$q_{sc,i}$	substrate conduction from heater element i (W/m^2)
q_{vap}	heat flux from heater to vapor FC-72 (W/m^2)
q_i	boiling heat transfer from heater element i (W/m^2)
$q_{total}(t)$	spatially averaged heat flux (W/m^2)
$\bar{q}_{total}$	time and spatially averaged heat flux (W/m^2)
ρ_l	liquid density (kg/m^3)
R_p	rms roughness of surface (m)
ρ_v	vapor density (kg/m^3)
s	1.7 for most liquids (1.0 for water)
σ	surface tension (N/m)
Δt	0.004 (s)
T	length of time average calculation (s)
T_{bulk}	bulk liquid temperature (C)
θ	contact angle (radians)
ΔT_{sub}	bulk liquid subcooling $= T_{sat} - T_{bulk}$ (C)
ΔT_{sat}	wall superheat $= T_w - T_{bulk}$ (C)
T_{sat}	saturated temperature (C)
T_w	wall temperature (C)

microconvection and not latent heat transport. For pool boiling near saturated conditions, Yaddanapuddi and Kim (2001) showed that during one ebullition cycle, the majority of heat transfer occurs after the bubble departs through transient conduction and microconvection to the rewetting liquid. Such results predict an increase in time average heat transfer for a corresponding increase in rewetting frequency. Methods aimed at increasing the bubble departure frequency, such as electro–hydrodynamic pool boiling, have clearly shown an increase in attainable heat flux. Baboi et al. (1968) observed that dielectrophoretic forces tend to increase CHF by increasing the rate of bubble departure. Snyder et al. (1998), while studying boiling from a platinum wire, observed an increase in nucleate boiling heat transfer and CHF in the presence of a strong electric field force co-linear with buoyancy. They concluded that the electric field acts to increase the forces acting on the bubbles promoting the rate of bubble departure. Such work characterizes the effect of two critical components of the ebullition cycle: the frequency of bubble departure or surface rewetting, f, and the bubble departure diameter, D_d.

The bubble departure diameter depends on the forces acting on the bubble during vapor bubble growth and departure. Surface tension, buoyancy, inertia of induced liquid motion, Marangoni or thermocapillary effects, and bulk fluid motion act to influence departure diameter. In addition, the magnitudes of these forces have been shown to be a function of bulk subcooling (ΔT_{sub}), gravity, wall superheat (ΔT_{sat}), the thermophysical properties of the fluid, heater geometry, surface characteristics, and pressure.

The frequency of bubble departure depends on the time needed for the bubble to grow to departure size (growth time) and the amount of time it takes after a bubble departs for nucleation to occur (waiting time). The bubble growth time in the nucleate boiling regime tends to decrease with wall superheat due to the increased rate of vapor generation which can cause an increase in bubble departure frequency. In addition, higher wall superheats tend to reduce the waiting time by decreasing the time needed for the bulk liquid to reach the superheat required for nucleation.

Many analytical models have been developed that predict nucleate boiling behavior in earth gravity from horizontal heaters significantly larger than the capillary length. A model developed by Fritz (1935), based on a quasistatic force balance between surface tension and buoyancy, assumes the non-dimensional Bond number

to be the governing parameter for bubble departure diameter. Additional models and correlations developed by Rohsenhow (1962), Eq. (2), Cooper (1984), Eq. (3), and Stephan and Abdelsalam (1980), provide an estimate of nucleate boiling heat transfer from relatively large heaters in earth gravity but fail to accurately account for boiling behavior across gravitational environments and at smaller scales.

$$\frac{q''}{(T_w - T_{sat})^3} C_{sf}^3 = \frac{\mu c_p^3}{h_{fg}^2 Pr^{3s}} \sqrt{\frac{g(\rho_l - \rho_v)}{\sigma}} \tag{2}$$

$$h = 55(q'')^{0.67} M^{-0.5} P_r^m (-\log_{10} P_r)^{-0.55} \tag{3}$$

Additionally, CHF models developed by Zuber (1959), Eq. (4), and Haramura and Katto (1983), quantify the mechanisms responsible for hydrodynamic instability assuming the non-dimensional Bond number, Bo, to be the governing parameter controlling the development of CHF in earth gravity.

$$q_{CHF} = \frac{\pi}{24} \rho_v h_{fg} \left(\frac{\sigma g(\rho_l - \rho_v)}{\rho_v^2} \right)^{1/4} \tag{4}$$

The correlations mentioned above do not accurately account for the gravitational dependence on boiling in low-g. For example, Merte et al. (1998) observed heat transfer that was higher in microgravity than in earth gravity at low heat flux. Kim et al. (2002) attributed bubble coalescence and primary bubble growth as the mechanism by which CHF occurs in low-g, which differs from the hydrodynamic instability model proposed by Zuber governing large horizontal surfaces. These findings and the work of DiMarco and Grassi (1999) show that boiling behavior cannot be cast solely in terms of the Bond number.

It has been observed (Forster and Greif, 1959) that subcooling has little to no effect on heat transfer during nucleate boiling in earth gravity. The combination of bubble departure frequency, liquid rewetting temperature, and the fraction of active nucleation sites acts to mitigate heat transfer differences across bulk subcoolings. Although negligible subcooling effects have been observed during nucleate pool boiling, bulk subcooling appears to significantly affect CHF. From a hydrodynamic perspective, an increase in subcooling acts to condense the vapor generated at the heated surface allowing bulk liquid to rewet the surface, delaying the onset of CHF. Kutateladze (1962) postulated that CHF in subcooled boiling should *increase* above similar saturated conditions by the amount of energy required to bring the subcooled liquid to a saturated state, Eq. (5). Ivey and Morris (1962) suggested $C_0 = 0.1$ and $n = 0.75$ based on available data.

$$\frac{q_{CHF,sub}}{q_{CHF,sat}} = 1 + C_0 \left(\frac{\rho_l}{\rho_v} \right)^n \frac{c_p(T_{sat} - T_{bulk})}{h_{fg}} \tag{5}$$

While extensive research has been conducted on heaters larger than the capillary length, less is known of boiling on the smaller scale and at lower gravity levels. Under low and microgravity conditions, the capillary length becomes very large raising questions about its scaling effectiveness. Analyzing the boiling mechanisms at the small scale, Bakhru and Lienhard (1972) studied boiling from small wires. Boiling curves presented in their work deviate significantly from classical boiling behavior in that no transitional boiling behavior from nucleate boiling to film boiling was observed and the formation of "patchy" boiling partially covered the wire. The Liedenfrost point and CHF were not observed in their study, leading to the conclusion that such regimes vanish for heater sizes smaller than $L_h/L_b < 0.01$. They concluded that classical pool boiling behavior is observed if the heater length is of the order $L_h/L_b > 0.15$. Additional studies of boiling on thin wires in low-g were performed by DiMarco and Grassi (1999). They report a boiling heat transfer coefficient to be largely unaffected by gravity level although bubble dynamics were strongly affected.

For flat horizontal heaters, experiments in low-g indicate the formation of a primary bubble that causes significant dryout over the heater surface. Under such conditions, bubble departure can be non-existent indicating that some of the bubble dynamics associated with the classical ebullition cycle no longer occur. Increased subcooling acts to reduce the size of the primary bubble causing, in some cases, bubble coalescence around the perimeter of the heater. Under highly subcooled conditions in low-g, it has been shown that for heater sizes where the primary bubble does not cause total dryout, bubble coalescence on the peripheral regions of the heater array causes similar heat transfer performance to classical 1-g nucleate boiling (Kim et al., 2002). Such findings lend support to the idea that if the primary bubble size can be predicted in low-g (0.01 g), earth gravity models and correlations might provide an accurate prediction of boiling behavior and total heat flux in low-g.

Thermocapillary or Marangoni convection has been shown to be a significant heat transfer mechanism in low-g at higher subcoolings. Temperature gradients along the vapor–liquid interface of the bubble cause surface tension induced convection which can act to hold growing bubbles on the heater surface. Although normally masked in 1-g by natural convection and bubble departure, thermocapillary convection becomes significant when coupled with reducing buoyant effects. Thermocapillary flow has been experimentally observed using interferometric techniques (Abe and Iwasaki, 1999).

While surface tension and primary bubble dynamics clearly dominate the boiling process in low-g, it also has been shown to dominate boiling at the small scale in

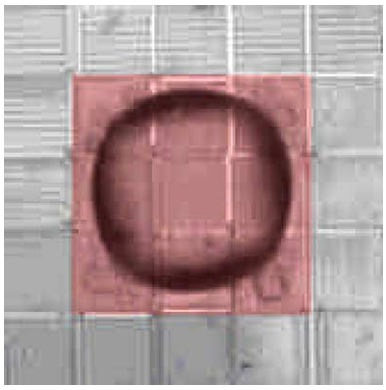

Fig. 1. Boiling on a 3×3-heater array (0.8 mm×0.8 mm) at 1.7-g, $\Delta T_{sub} = 31$ °C, $\Delta T_{sat} = 34$ °C.

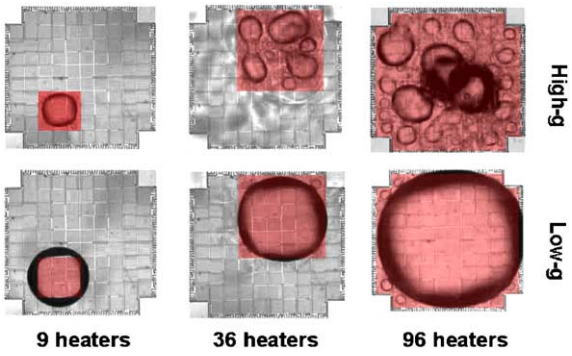

Fig. 2. Boiling on heaters of various size in low-g and high-g, $T_{bulk} = 28$ °C, $\Delta T_{sat} = 34$ °C.

high-g. Recent work performed by Kim and Henry (2003) shows high-g boiling on small heaters (0.8 mm×0.8 mm), where $L_h/L_b = 1.5$, can be surface tension dominated forming a stable primary bubble, as shown in Fig. 1, similar to boiling in low-g. They proposed that the transition from buoyancy to surface tension dominated boiling occurred when the bubble departure diameter and the heater size are on the same order, as seen in Fig. 2. Over the gravity levels where the primary bubble departed, the departure frequency was observed to decrease with increased subcooling due to enhanced condensation at the bubble cap. In this paper, the effects of heater size, subcooling, and gravity level on pool boiling heat transfer is presented through photographic and quantitative results.

2. Experimental appartus

Local heat flux measurement and temperature control were performed using an array of platinum resistance heater elements deposited on a quartz wafer in a serpentine pattern. Each of these elements was 0.27 mm×0.27 mm in size, had a nominal resistance of 1000 Ω, and a nominal temperature coefficient of resistance of

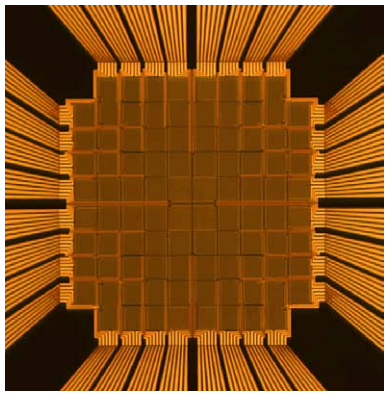

Fig. 3. Platinum resistance heater array, each heater element = 0.27 mm×0.27 mm.

0.002 °C^{-1}. The heater consisted of ninety-six individual heaters arranged in a square array approximately 2.7 mm on a side, Fig. 3. The reader is referred to Rule and Kim (1999) for details of the heater construction.

2.1. Electronics

The temperature of each heater in the array was kept constant by a bank of feedback circuits similar to those used in constant temperature hot-wire anemometry. The electronics provided temperature control over the range 20–125 °C ± 1 °C after calibration. The electronics used in this experiment were similar to those used in previous experiments and are described in Bae et al. (1999). The transient voltage across each individual heater was sampled by a data acquisition system with a maximum sample rate of 500 Hz.

2.2. Payload

A schematic of the boiling rig used in this study is shown in Fig. 4. The bellows and the surrounding housing allowed the test section pressure to be controlled. A pump was used to break up thermal stratification within the test chamber, while a PID temperature controller, a thermistor, and thin film heaters attached to the boiling chamber were used to control the bulk fluid temperature. A pressure transducer rated at 200 psia was used to measure the pressure at the heater surface.

The test chamber was filled with nominally 3 liters of distilled FC-72 ($T_{sat} = 56.7$ °C at 1 atm). The fluid was degassed by periodically reducing the pressure with a vacuum pump allowing dissolved gases to diffuse out of the liquid. Degassing was performed over several days ensuring minimal gas concentrations. The final dissolved gas concentration in the liquid (determined using the chamber temperature and pressure, the thermophysical properties of FC-72, and Henry's law) was less than 1.5×10^{-3} moles/mole. Gas concentrations smaller than

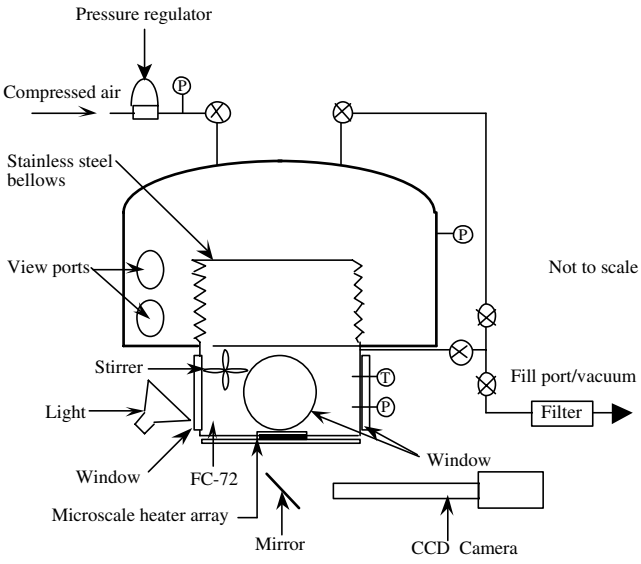

Fig. 4. Schematic of test rig.

2×10^{-3} moles/mole have been shown to have no influence on the boiling behavior (You et al., 1995) in earth gravity. However, it has been argued that the presence of even minute amounts of dissolved gas can cause formation of thermocapillary convection around vapor bubbles in subcooled, low-g environments (Straub, 2002). Strong Marangoni convection was observed in the present data at high subcoolings. Unfortunately, very little information is currently available regarding the influence of thermocapillary convection on boiling heat transfer in microgravity, and consequently the extent to which the data was influenced by the small amount of dissolved gas is unknown.

The heater array was cooled from the bottom using an air jet at ambient temperature with a flow rate of 230 cm^3/s through a 1.6 mm ID diameter nozzle to prevent individual heaters from shutting off at low heat transfer levels (such as occurs when a large bubble covers the heater). The heat flux associated with air jet cooling was subtracted from the heat flux signal during data reduction to determine the actual heat transfer from the heater surface to the liquid.

Side windows and the transparent characteristics of the heater array allowed for images to be taken of the boiling from the bottom and side. Two 29.97 Hz CCD cameras and mini-DV camcorders were used for this purpose. Acceleration data in the direction perpendicular to the floor of the aircraft was obtained using one axis of an accelerometer (Entran EGCS3) with a sensitivity of 2.5 V/g and a frequency response of 0–90 Hz. Accelerometer, pressure, and the output voltage of the heater array were sampled at 250 Hz.

The heater array was calibrated using a constant temperature oven. PID temperature controllers, two thermocouples, and two thin film heaters were used to maintain a constant temperature environment within the oven. The heater was allowed to equilibriate within the oven for 2 h before each calibration. For additional comments on the calibration procedure, the reader is referred to Bae et al. (1999).

2.3. Test procedure

Data presented in this paper were taken aboard the NASA KC-135 over a three week period totaling 10 flights. During a portion of the parabolic flight, low-g levels (0.01 g) were produced, and a typical flight consisted of 40 parabolic maneuvers. Each parabolic maneuver consisted of a high-g pullup (1.8 g), a low-g period of about 25 s, followed by a high-g pullout (1.6–1.7 g). Data acquisition for a particular wall temperature was initiated during the transition from high-g to low-g. Data were obtained for 90 s throughout the entire low-g period and into the high-g pullout and pullup. The pump was turned on during turns (every eighth parabola) providing turbulent mixing that minimized temperature gradients within the bulk liquid. Data were obtained for 9 (3×3, 0.65 mm^2), 36 (6×6, 2.62 mm^2) and 96 (7.29 mm^2) heaters powered for bulk fluid temperatures of 28, 35, 45, and 55 °C. The wall temperature was varied from 70 to 105 °C in 5 °C increments. Because the bulk temperature could take up to 2 hours to stabilize, one set of data at a given bulk temperature was obtained per flight. The order in which data were obtained on a given day at various wall superheats and heater sizes was randomized.

3. Data reduction and uncertainty analysis

Data analysis was performed using a Matlab routine. The transient output voltage of each heater in the array was used with its corresponding resistance and area to effectively measure the transient heat flux supplied to each heater element ($q_{\mathrm{raw},i}$). Heater resistances were measured during the calibration process using a multimeter to obtain an accurate value for calculating the power dissipated by the heater while providing a reliable measurement of the temperature coefficient of resistance for each heater element.

The amount of heat transferred to the boiling liquid (q_i) was calculated by subtracting the heat flux dissipated through the quartz heater substrate, $q_{\mathrm{sc},i}$, from $q_{\mathrm{raw},i}$. The magnitude of $q_{\mathrm{sc},i}$ was determined by locating relatively long time periods during which vapor totally covered a heater (such as occurs when a large bubble causes dryout over a heater at low bulk subcoolings) in low-g and attributing the heat flux at this time to substrate conduction. During such times, the heat transfer from the wall to the vapor was very low due to the comparatively low thermal conductivity of FC-72 vapor

compared to that of quartz. Assuming a vapor thermal conductivity equal to that of the liquid, a vapor layer thickness of 0.5 mm, and a maximum temperature difference to be equal to the maximum wall superheat tested (47 °C), a conservative estimate of $q_{vap} = 0.5$ W/cm^2 was obtained. This value was on the order of the uncertainty in the total heat flux measurement and is an order of magnitude smaller than calculated substrate conduction values. The radiation between the wall and liquid was negligible compared to the substrate conduction. All heat transferred to the liquid during times when local dryout occurs was assumed negligible.

Typical experimental distributions of $q_{sc,i}$ on the heater array are shown in Fig. 5. Higher substrate conduction values are observed near the corner and edge heaters due to the increased area for lateral conduction to the substrate. Numerical modeling of the substrate conduction was also performed and the results agreed to within 10% of the experimental values. Such results provide a good estimate of the uncertainty in $q_{sc,i}$. A propagation of uncertainty analysis, accounting for additional errors in the hardware measurements, yielded an uncertainty in q_i of ±12%.

Boiling heat transfer data was taken from data obtained in high-g and low-g where the heat transfer had reached steady state (in each respective environment) over an interval of 5 s to 10 s where the g-levels were within ±0.025 g and ±0.5 g respectively. Spatially averaged, time resolved heat flux data were obtained using the following equation:

$$q_{total}(t) = \frac{\sum_{i=1}^{n}[q_{raw,i}(t) - q_{sc,i}]A_i}{\sum_{i=1}^{n} A_i} \quad (6)$$

where the subscript i denotes the heaters and n is the total number of powered heaters. A typical $q_{total}(t)$ is given in Fig. 6, and shows the variation in heat transfer during the low-g and high-g environments. The space and time averaged heat flux were obtained using:

$$\bar{q}_{total} = \frac{\sum_{j=1}^{T} q_{total}(t)\Delta t}{T} \quad (7)$$

where Δt is the time between data points and T is the total time over which the average is obtained.

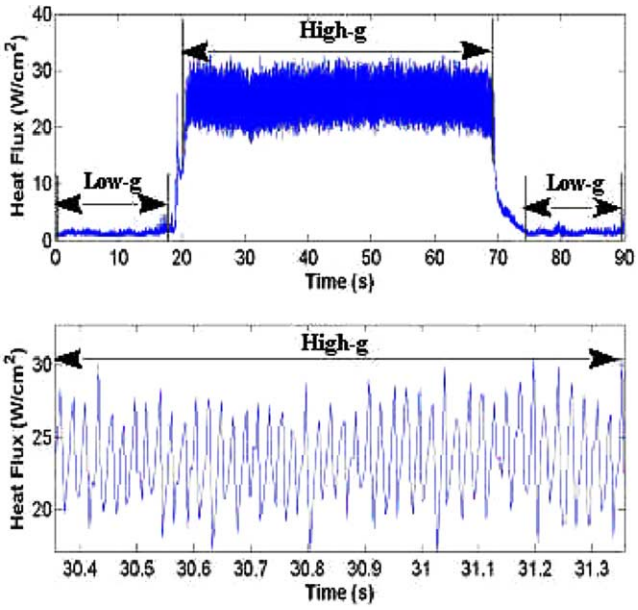

Fig. 6. Spatially averaged and time resolved heat flux trace (heat flux trace at a smaller time scale, bottom).

Uncertainties associated with the wall superheat and subcooling level occur due to uncertainties in heater calibration (2 digital potentiometer settings or ±0.68 °C), uncertainties associated with measurement of bulk fluid temperature, T_{bulk}, and pressure errors. The thermistor used to measure the fluid temperature and the RTD used to control the chamber sidewall temperature were calibrated in a constant temperature water bath using a NIST traceable liquid-in-glass thermometer. The saturation temperature of the fluid, T_{sat}, was calculated from a measurement of the time resolved pressure at the heater surface and the saturation curve data as presented in the 3M catalog (3M, 1995). Hydrostatic pressure changes due to the vertical position of the pressure transducer were also accounted for. The uncertainties associated with ΔT_{sub} and ΔT_{sat} were both ±1 °C.

The liquid rewetting frequency in high-g was determined from $q_{total}(t)$. For example, times when a peak in heat transfer occurs in Fig. 6 (bottom) are thought to correspond to bulk liquid rewetting the heater surface.

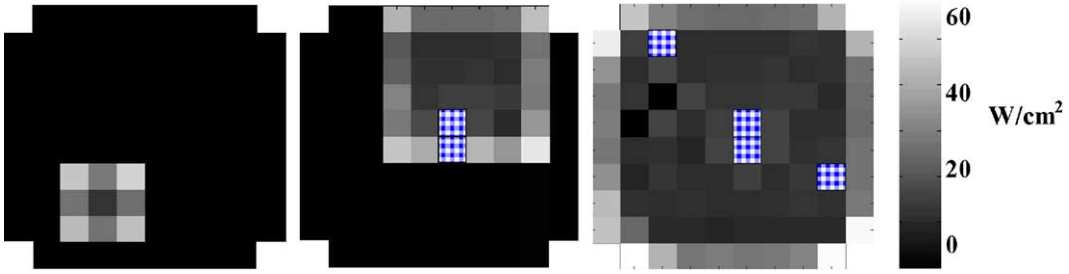

Fig. 5. Typical substrate conduction (W/cm^2) from a 9-, 36-, and 96-heater array, $T_{bulk} = 55$ °C, $T_w = 90$ °C. Non-functional heaters on the 36- and 96-heater arrays are checkered.

The number of heat flux peaks per unit time was taken to be the average rewetting frequency. For frequencies well below the video framing rate (29.97 Hz), the rewetting frequency as computed above agreed well with the primary bubble departure frequency obtained from the video. For the 9 and 36 heater array, the formation of a bubble was clearly observed across gravitational levels. For the 96-heater array, a distinct primary bubble was not observed at higher gravity levels and therefore primary bubble dynamics no longer strongly affected the boiling behavior. Primary bubble formation and growth of a dry area on the surface is believed to cause a reduction in heat transfer. Primary bubble departure did not occur in low-g, as indicated by the relatively low heat transfer and the absence of distinct peaks in Fig. 6.

4. Results

The saturation temperatures for each g-level were calculated based on the measured liquid pressure at the heater surface and the thermophysical properties of the fluid. For higher bulk temperatures, the pressure within the chamber increased slightly above atmospheric pressure increasing the saturation temperature of the fluid. Table 1 summarizes the conditions studied.

4.1. Low gravity boiling characteristics

Nine-heater array. Images of the boiling behavior for a 9-heater array are shown in Fig. 7 and the corresponding boiling curves in low-g are presented in Fig. 8. For the 9-heater array, a primary bubble was observed

Table 1
Summary of test conditions for each flight

Flight no.	T_{bulk} (°C)	Saturation temperature (°C) [subcooling level (°C)]	
		Low-g	High-g
1	35.0	58.1 [23.1]	59.9 [24.9]
2	54.8	61.2 [6.4]	62.8 [8.0]
3	45.3	59.7 [14.4]	61.3 [16.0]
4	28.4	57.2 [28.8]	59.6 [31.2]

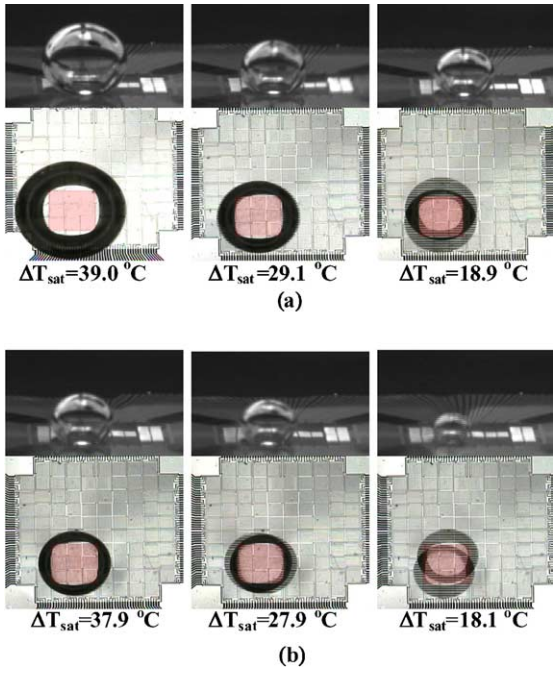

Fig. 7. Boiling pictures (bottom and side view) from a 9-heater array in low-g. (a) $\Delta T_{sub} = 6$ °C, $T_{bulk} = 55$ °C. (b) $\Delta T_{sub} = 29$ °C, $T_{bulk} = 28$ °C.

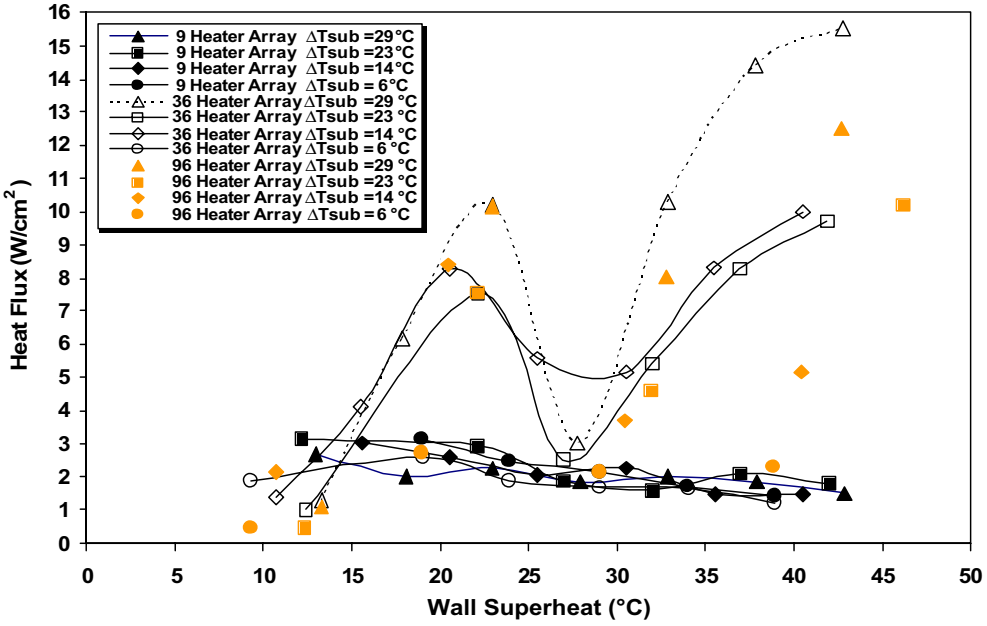

Fig. 8. Boiling curves in low-g (0.01 g) for different heater sizes and subcoolings.

to form and cause dryout over significant portions of the heater surface. Subcooling was found to have little effect on the size of the dry area, and may explain why the boiling curves are not affected by subcooling. At low wall superheats, the primary bubble oscillated laterally on the surface, and allowed rewetting to occur over a portion of the heater surface. The cause of such oscillations is currently unknown but may be due to g-jitter or thermocapillary forces. The magnitude of oscillations decreased with increasing wall superheat and the dry area size increased, resulting in a lower average heat flux. CHF appeared to occur at very low superheats immediately following boiling incipience.

Thirty six-heater array. For the 36-heater array in low-g the boiling process was again dominated by the primary bubble. Boiling curves in low-g for a 36-heater array are shown in Fig. 8. At low subcoolings ($\Delta T_{sub} = 6$ °C, Fig. 9a), nearly complete heater dryout occurred, and boiling performance was relatively constant and characteristically low over the superheats studied. At higher subcoolings, the primary bubble becomes significantly smaller. Consider first the highest subooling tested ($\Delta T_{sub} = 29$ °C), Fig. 10(a). At low superheats, the primary bubble is significantly smaller than the heater size and few active nucleation sites are observed. The rapid increase in wall heat transfer as the superheat increases to 23 °C (CHF) is due to an increase in the number of active nucleation sites (the images shown in Fig. 10 are interlaced which conveys the magnitude of bubble velocity). Coalescence with the primary bubble

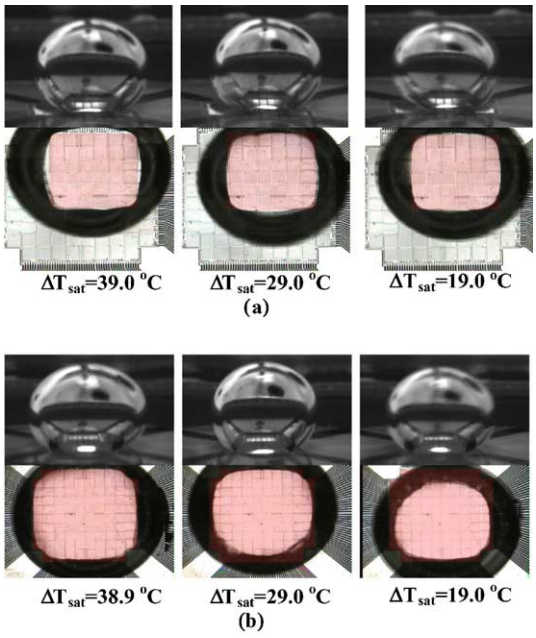

Fig. 9. Boiling pictures (bottom and side view) from 36 (a) and 96 (b) heater arrays in low-g. (a) 36-heater array, $\Delta T_{sub} = 6$ °C, $T_{bulk} = 55$ °C. (b) 96-heater array, $\Delta T_{sub} = 6$ °C, $T_{bulk} = 55$ °C.

was observed to be the satellite bubble removal mechanism. As the superheat is increased above CHF to 28 °C, a sharp decrease in heat transfer occurs due to increased dryout of the heater. As the superheat was increased above 32 °C, a strong increase in thermocapillary convection was observed. This resulted in a

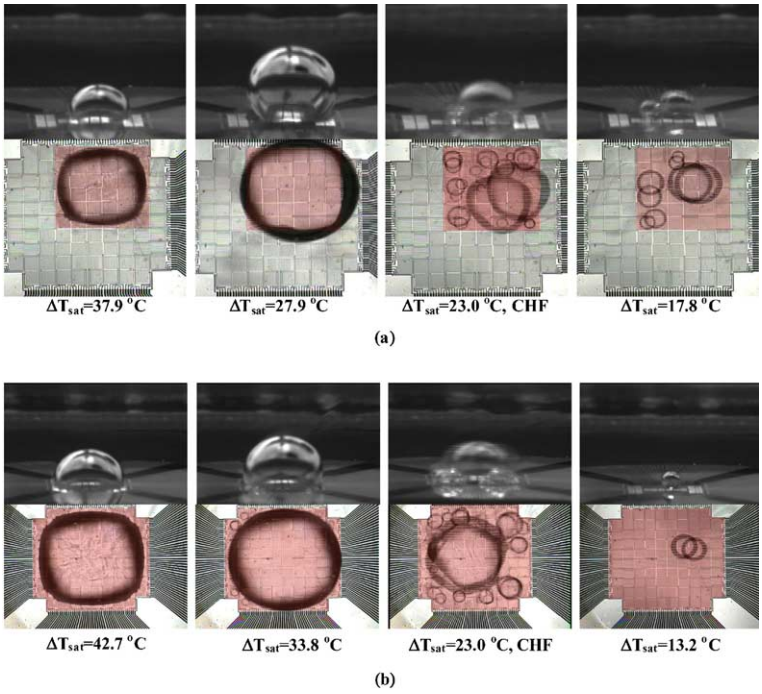

Fig. 10. Boiling pictures (bottom and side view) from 36 (a) and 96 (b) heater arrays in low-g. (a) 36-heater array, $\Delta T_{sub} = 29$ °C, $T_{bulk} = 28$ °C. (b) 96-heater array, $\Delta T_{sub} = 29$ °C, $T_{bulk} = 28$ °C.

decrease in the primary bubble size by increasing the rate of condensation at the bubble cap, and allowed increasing satellite bubble formation and an enhancement in heat transfer. As seen in Fig. 8, the heat flux at this superheat is 50% larger than CHF. The trend in the boiling curve at this point indicates that a second local maximum heat flux may exist in low-g. Further experimentation is necessary to validate such trends. The mechanism by which thermocapillary convection develops in nominally pure fluids is still unclear, but may be related to the presence of dissolved gases in the liquid, as suggested by Straub (2002). Similar trends in the heat transfer data are observed for the $\Delta T_{sub} = 23$ °C and $\Delta T_{sub} = 14$ °C cases.

Ninety six-heater array. Boiling curves for the 96-heater array in low-g are shown in Fig. 8. Images of the boiling behavior are shown in Figs. 9(b) and 10(b). For the 96-heater array, trends similar to those for the 36-heater array are observed. At low subcoolings ($\Delta T_{sub} = 6$ °C), heater dryout caused the boiling heat flux to be relatively small. At higher subcoolings, the size of the primary bubble decreased resulting in an increase in satellite bubble formation. Coalescence was again observed to be the primary mechanism for CHF at higher subcoolings, similar to the 36-heater array. Although strong thermocapillary convection was observed at high subcoolings and high superheats, data was not obtained with sufficient superheat resolution to determine whether a local maximum occurs after CHF.

In summary, low-g boiling behavior is governed by the dynamics of the primary bubble. For the 9-heater array, total dryout of the heater occurs over the subcooling ranges studied. For larger heaters, increased subcooling decreased the size of the primary bubble, allowing satellite bubbles to form with a corresponding increase in heat transfer. CHF appeared to be a result of the competition between increasing heat transfer associated with the satellite bubbles and the decrease in heat transfer due to growth of the dry area under the primary bubble as the wall superheat increases. Thermocapillary convection may be responsible for the post-CHF increase in heat flux observed in the 36- and 96-heater cases at higher subcoolings.

4.2. High gravity boiling characteristics

Nine-heater array. Boiling curves for the 9-heater array in high-g are presented in Fig. 11. Images of the boiling behavior for a 9-heater array in high-g are shown in Fig. 12. At low wall superheats, the images show few active nucleation sites. At higher superheats, the images clearly indicate the formation of a primary bubble surrounded by satellite bubbles, similar to what is observed in low-g for larger heaters. No primary bubble departure was observed except for one case ($\Delta T_{sat} = 37.3$ °C, $\Delta T_{sub} = 8$ °C) in which departure was infrequent (<1 Hz). Surface tension clearly dominated the boiling dynamics over the superheat and subcooling ranges tested. Coalescence of the satellite bubbles with the primary bubble, surface tension, and increased condensation at the cap of the bubble due to natural convection prevented the primary bubble from reaching the size required for departure. The primary bubbles in high-g were seen to be significantly smaller than those

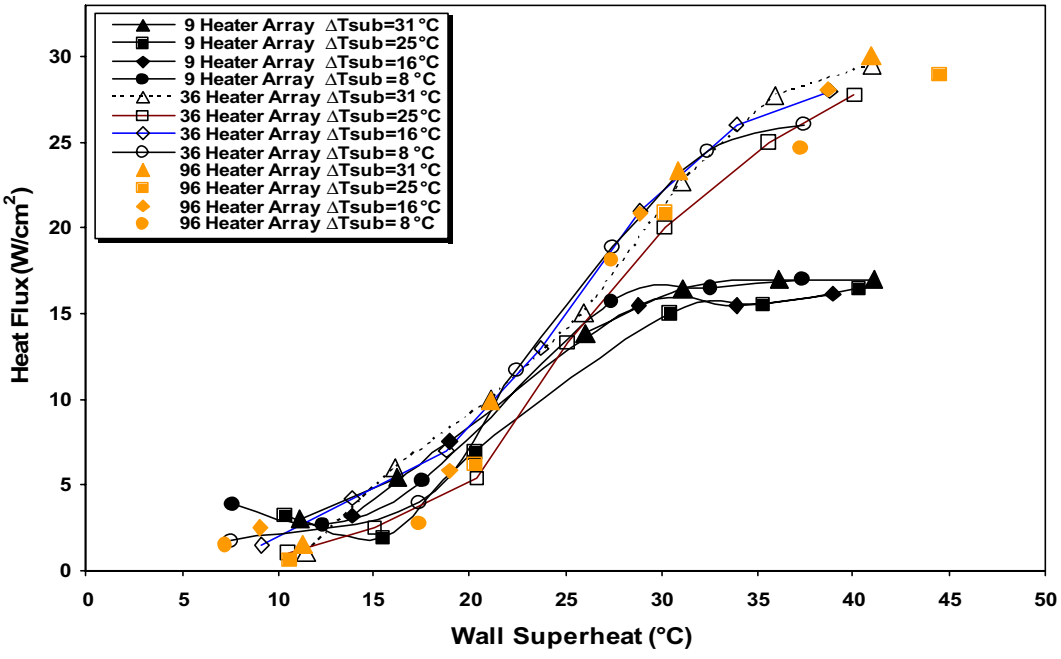

Fig. 11. Boiling curves in high-g for different heater sizes and subcoolings.

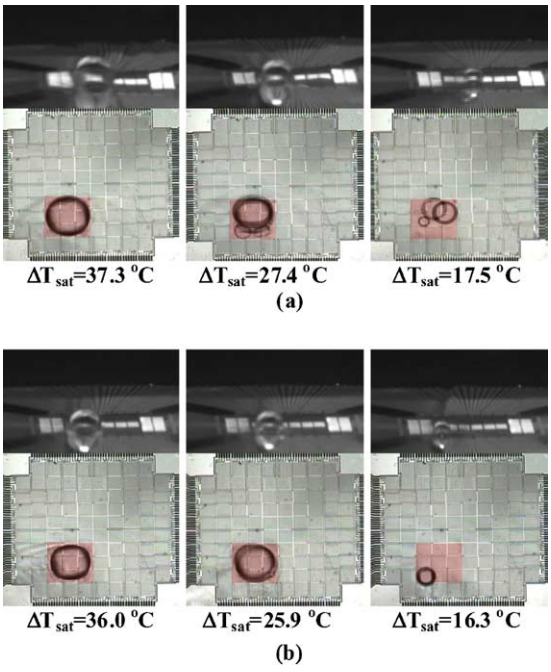

Fig. 12. Boiling pictures (bottom and side view) from a 9-heater array in high-g. (a) $\Delta T_{sub} = 8$ °C, $T_{bulk} = 55$ °C. (b) $\Delta T_{sub} = 31$ °C, $T_{bulk} = 28$ °C.

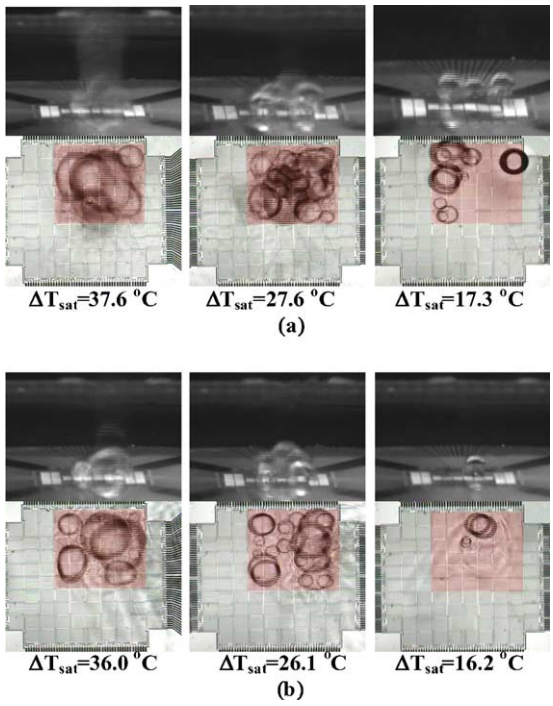

Fig. 13. Boiling pictures (bottom and side view) from a 36-heater array in high-g. (a) $\Delta T_{sub} = 8$ °C, $T_{bulk} = 55$ °C. (b) $\Delta T_{sub} = 31$ °C, $T_{bulk} = 28$ °C.

observed in low-g. The high heat fluxes observed in Fig. 11 compared to those in low-g for larger heaters are a direct result of the smaller primary bubble size which allows an increase in the area over which satellite bubble formation can occur. Increased subcooling was seen to have a negligible effect on heat transfer over the ranges tested. The heat transfer from the array at higher superheats again appears to be the result of competition between increasing heat transfer associated with the satellite bubbles and the decrease in heat transfer due to growth of the dry area under the primary bubble.

Thirty six-heater array. Boiling curves for the 36-heater array are shown in Fig. 11. Primary bubble formation was again witnessed at higher wall superheats and higher bulk subcoolings. Fig. 13 shows high-g boiling behavior for various wall superheats and bulk subcoolings. The primary bubble that formed in high-g was pulled off the heater array periodically, allowing the entire heater to be rewetted with liquid. The size of the primary bubble was smaller for higher subcoolings, as observed for the 9-heater case and the low-g cases. The heat fluxes at lower superheats were very similar to those observed for the 9-heater array. At higher superheats, the subcooling level appears to have a negligible affect on heat flux, contrary to many previous studies which indicate an increase in the heat transfer with increased subcooling near CHF.

Although the subcooling level had a negligible affect on time and space averaged heat flux, increased subcooling was shown to dramatically reduce the departure frequency of the primary bubble as shown on Fig. 14.

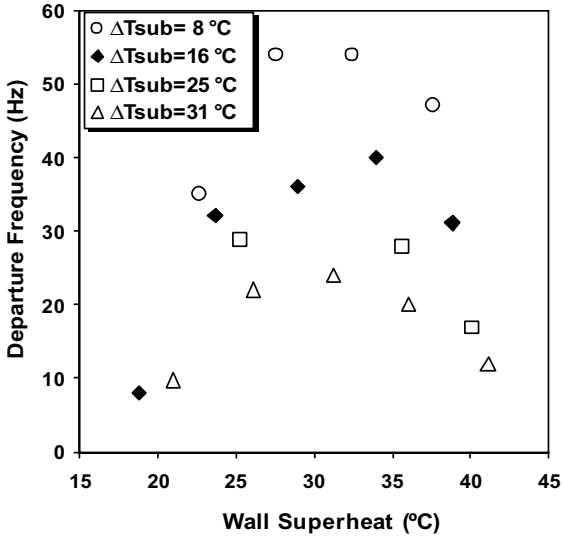

Fig. 14. Primary bubble departure frequency in high-g for a 36-heater array.

The departure frequency was determined from $q_{total}(t)$, as discussed in the data reduction section. The bubble departure frequency increased by over 100% as the bulk subcooling decreased from $\Delta T_{sub} = 31$ °C to $\Delta T_{sub} = 8$ °C at a superheat of 32 °C. Increased subcooling increased condensation from the cap of a growing primary bubble reducing its growth rate. The longer time needed for the bubble to reach departure size resulted in a

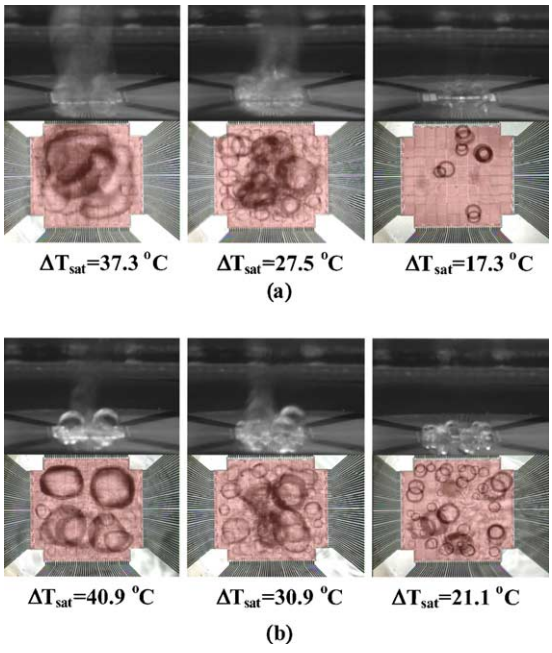

Fig. 15. Boiling pictures (bottom and side view) from a 96-heater array in high-g. (a) $\Delta T_{sub} = 8$ °C, $T_{bulk} = 55$ °C. (b) $\Delta T_{sub} = 31$ °C, $T_{bulk} = 28$ °C.

decreased departure frequency which decreased time-averaged heat transfer. It appears this effect is compensated for by the larger temperature difference between the wall and the bulk liquid. The effect on CHF observed by other researchers and models, e.g. Kutateladze (1962) is clearly not observed in Fig. 11. As mentioned previously, the Bond number and capillary length have been used as scaling parameters for many boiling heat transfer models. Additional parameters accounting for heater size and gravity are clearly needed in future prediction models.

Ninety six-heater array. Boiling curves for a 96-heater array in high-g are shown in Fig. 11. Pictures of boiling are shown in Fig. 15. Nucleate boiling without primary bubble formation was observed at all subcooling and superheats except for those corresponding to $\Delta T_{sat} \sim 40$ °C. At this temperature, the beginning of a primary bubble was observed for $\Delta T_{sub} = 16$ °C and $\Delta T_{sub} = 8$ °C. For $\Delta T_{sub} = 31$ °C and $\Delta T_{sub} = 25$ °C, the primary bubble fractured into four primary bubbles (e.g., Fig. 15(b), $\Delta T_{sat} = 40.9$ °C).

5. Conclusions

At low wall superheats ($\Delta T_{sat} < 18$ °C), boiling performance appears to be constant across gravity levels. At higher wall superheats, boiling performance is significantly reduced in low-g due to heater dryout and the reduction of bubble removal forces such as buoyancy. Increased subcooling appears to delay the degradation in boiling performance (compared to high-g) to higher wall superheats. In low-g, a reduction in heater size appears to decrease satellite bubble formation. In addition, the heater size appears to strongly affect thermocapillary induced heat transfer that occurs post CHF. In high-g, heater size appears to strongly affect bubble departure frequency by placing limitations on the size of a growing bubble.

In summary, it appears that the size of the primary bubble relative to the heater size determines the heat transfer. The wall superheat, heater size, subcooling, and the development of thermocapillary convection all impact the size of the bubble that forms.

5.1. Low-g

(1) CHF increases with subcooling if the dry area under the primary bubble is smaller than the heater array (36- and 96-heater arrays). Subcooling does not affect small heaters (9-heater array).
(2) CHF appears to be a result of a competition between increasing heat transfer associated with the satellite bubbles and the decrease in heat transfer due to growth of the dry area under the primary bubble.
(3) Thermocapillary convection at higher superheats and subcoolings can decrease the size of the primary bubble, resulting in an increase in heat transfer above CHF.

5.2. High-g

(1) Boiling on the 9-heater array was very similar to boiling on larger heaters in low-g. A primary bubble forms on the heater that departs infrequently. This primary bubble is significantly smaller that the one that forms in low-g, allowing liquid to wet the peripheral regions of the heater surface providing a relatively higher heat transfer.
(2) For the 36- and 96-heater cases, increased subcooling decreases primary bubble departure frequency which tends to reduce the time-averaged heat transfer. This effect is compensated for by the larger temperature difference between the wall and the bulk fluid which increases the heater transfer.

Acknowledgements

This work was supported by the Office of Biological and Physical Research at NASA Headquarters. The grant monitor was Mr. John McQuillen.

References

Abe, Y., Iwasaki, A., 1999. Single and dual vapor bubble experiments in microgravity, Proceeding of the Microgravity Fluid Physics and Heat Transfer Conference, 19–24 September, Kahuku, Hawaii.

Baboi, N.F., Bologa, M.K., Klyukanov, A.A., 1968. Some features of ebullition in an electric field. Appl. Electr. Phenom. 20, 57–70, USSR.

Bae, S., Kim, M., Kim, J., 1999. Improved technique to measure time- and space-resolved heat transfer under single bubbles during saturated pool boiling Of FC-72. Experimental Heat Transfer 12 (3), 265–278.

Bakhru, N., Lienhard, J.H., 1972. Boiling from small cylinders. Int. J. Heat Mass Transfer 15, 2011–2025.

Cooper, M.G., 1984. Saturation nucleate, pool boiling—a simple correlation. Inst. Chem. Engr. Symp. Ser. 86, 785–792.

DiMarco, P., Grassi, W., 1999. About the scaling of critical heat flux with gravity acceleration in pool boiling, XVII UIT National Heat Transfer Conference, Ferrara, June 30–July 2.

Forster, H.K., Greif, R., 1959. Heat transfer to a boiling liquid—mechanisms and correlations. J. Heat Transfer 81, 45.

Fritz, W., 1935. Berechnungen des Maximalvolumens von Dampfblasen. Phys. Z. 36, 379–384.

Gunther, F.C., Kreith, F., 1956. Photographic Study of Bubble Formation in Heat Transfer to Subcooled Water, Prog. Rept. 4-120, Jet Propulsion Lab., California Institute of Technology, Pasadena, CA, March.

Haramura, Y., Katto, Y., 1983. A new hydrodynamic model of the critical heat flux, applicable widely to both pool and forced convective boiling on submerged bodies in saturated liquids. Int. J. Heat Mass Transfer 26, 389–399.

Ivey, H.J., Morris, D.J., 1962. On the relevance of the vapor–liquid exchange mechanism for subcooled boiling heat transfer at high pressure. British Rep. AEEW-R-137, Atomic Energy Establishment, Winfrith.

Kim, J., Henry, C.D., 2003. Heater size and gravity effects on pool boiling heat transfer. Am. Inst. Phys. Conf. Proc. 654, 132–141.

Kim, J., Benton, J.F., Wisniewski, D., 2002. Pool boiling heat transfer on small heaters: effect of gravity and subcooling. Int. J. Heat Mass Transfer 45, 3919–3932.

Kutateladze, S.S., 1962. Heat Transfer During Condensation and Boiling, translated from a publication of the State Scientific and Technical Publishers of Literature and Machinery, Moscow-Leningrad, as AEC-TR-3770.

Merte, H., Lee, H.S., Keller, R.B., 1998. Dryout and Rewetting in the Pool Boiling Experiment Flown on STS-72 (PBE-IIB) and STS-77 (PBE-IIA). NASA Report #E-11185.

Rohsenhow, W.M., 1962. A method of correlating heat transfer data for surface boiling of liquids. Trans. ASME 84, 969.

Rule, T.D., Kim, J., 1999. Heat transfer behavior on small horizontal heaters during pool boiling of FC-72. J. Heat Transfer 121 (2), 386–393.

Snyder, T.J., Chung, J., Schneider, J., 1998. Competing effects of dielectrophoresis and buoyancy on nucleate boiling and an analogy with variable gravity boiling results. J. Heat Transfer 120, 371–379.

Stephan, Abdelsalam, 1980. Heat transfer correlations for natural convection boiling. Int. J. Heat Mass Transfer 23, 73–87.

Straub, J., 2002. Origin and effect of thermocapillary convection in subcooled boiling: observations and conclusions from experiments performed at microgravity. Ann. New York Acad. Sci. 974, 348–363.

Yaddanapuddi, N., Kim, J., 2001. Single bubble heat transfer in saturated pool boiling of FC-72. Multiphase Sci. Technol. 12 (3–4), 47–63.

You, S.M., Simon, T.W., Bar-Cohen, A., Hong, 1995. Effect of dissolved gas content on pool boiling of a highly wetting fluid. J. Heat Transfer 117, 687–692.

Zuber, N., 1959. Hydrodynamics of Boiling Heat Transfer. AEC Report AECU-4439.